APTO-253 Is a New Addition to the Repertoire of Drugs that Can Exploit DNA BRCA1/2 Deficiency

Cheng-Yu Tsai[1], Si Sun[1], Hongying Zhang[2], Andrea Local[2], Yongxuan Su[3], Larry A. Gross[3], William G. Rice[2], and Stephen B. Howell[1,4]

Abstract

APTO-253 is a small molecule with antiproliferative activity against cell lines derived from a wide range of human malignancies. We sought to determine the mechanisms of action and basis for resistance to APTO-253 so as to identify synthetic lethal interactions that can guide combination studies. The cellular pharmacology of APTO-253 was analyzed in Raji lymphoma cells and a subline selected for resistance (Raji/253R). Using LC/MS/ESI analysis, APTO-253 was found to convert intracellularly to a complex containing one molecule of iron and three molecules of APTO-253 [$Fe(253)_3$]. The intracellular content of $Fe(253)_3$ exceeded that of the native drug by approximately 18-fold, and $Fe(253)_3$ appears to be the most active form. Treatment of cells with APTO-253 caused DNA damage, which led us to ask whether cells deficient in homologous recombination (i.e., loss of BRCA1/2 function) were hypersensitive to this drug. It was found that loss of either BRCA1 or BRCA2 function in multiple isogenic paired cell lines resulted in hypersensitivity to APTO-253 of a magnitude similar to the effects of PARP inhibitors, olaparib. Raji cells selected for 16-fold acquired resistance had 16-fold reduced accumulation of $Fe(253)_3$. RNA-seq analysis revealed that overexpression of the ABCG2 drug efflux pump is a key mechanism of resistance. ABCG2-overexpressed HEK-293 cells were resistant to APTO-253, and inhibition of ABCG2 reversed resistance to APTO-253 in Raji/253R. APTO-253 joins the limited repertoire of drugs that can exploit defects in homologous recombination and is of particular interest because it does not produce myelosuppression. *Mol Cancer Ther; 17(6); 1–10. ©2018 AACR.*

Introduction

A precursor molecule of APTO-253 that killed cancer cells was discovered in a small molecule screen of novel indolyl-phenanthroline-imidazoles. Phenanthrolines are known to form complexes with several doubly charged metals like Fe, Zn, and Ru, and these metal complexes bind to calf thymus DNA with varying binding constants (1–4). Further chemical modification of the precursor to optimize anticancer activity yielded the novel compound APTO-253. APTO-253 was subsequently shown to have activity against cell lines derived from a wide range of human malignancies, including leukemias, lymphomas, colon, and non–small cell lung carcinomas with IC_{50} values ranging from approximately 0.04 to 2.6 µmol/L. When tested *in vivo* in murine xenograft models, APTO-253 produced antitumor responses in the human HT-29 colon adenocarcinoma (5), H460 non–small cell lung cancer, H226 squamous cell carcinoma/mesothelioma (6), and KG1 acute myelogenous leukemia (AML) xenografts when administered by the intravenous route. Toxicology studies disclosed no evidence of myelosuppression.

APTO-253 was advanced into a phase I trial in patients with solid tumors (7). The drug was administered intravenously on days 1 and 2, and 15 and 16 of each 28-day cycle, and the dose was escalated from 20 to 387 mg/m^2 in 9 cohorts. Thirty-two patients were treated in this trial, and fatigue was the only drug-related treatment-emergent adverse event to occur in >10% of patients. Dose-limiting toxicities of hypersensitivity reaction and transient hypotension despite prophylaxis occurred at 387 mg/m^2, which led to identification of 298 mg/m^2 as the MTD. APTO-253 was well tolerated at the phase II recommended dose and produced evidence of antitumor activity in the form of stable disease in 5 of the 21 evaluable patients (23.8 %) with durations ranging from 3.6 to 8.4 months.

The structure of APTO-253 (Fig. 1A) suggested that it can chelate Zn and Fe and potentially bind to DNA. APTO-253 was later found to cause cell-cycle arrest in G_0–G_1, and in both leukemic and solid tumor cell lines, the primary route of cell death is apoptosis (5, 8–10). More extensive studies in human AML disclosed upregulation of CDKN1A and, most importantly, that APTO-253 downregulates the expression of Myc in both a concentration- and time-dependent manner (9). Through the auspices of the BEAT AML Project (http://www.lls.org/beat-aml), APTO-253 has now been tested *in vitro* for activity against 177 freshly isolated bone marrow samples from patients with AML, chronic lymphocytic leukemia (CLL), or myelodysplasia

[1]Moores Cancer Center, San Diego, California. [2]Aptose Biosciences, Inc, San Diego, California. [3]Department of Chemistry and Biochemistry, University of California, San Diego, California. [4]Department of Medicine, University of California, San Diego, California.

Current address for S. Sun: Department of Obstetrics and Gynecology, Union Hospital, Tongji Medical College, Huazhong University of Science and Technology, Wuhan 430022, China.

Corresponding Author: Stephen B. Howell, University of California, San Diego, 3855 Health Sciences Drive, Mail Code 0819, La Jolla, CA 92093-0819. Phone: 858-822-1110; Fax: 858-822-1111; E-mail: showell@ucsd.edu

(MDS)/myeloproliferative disorders (MPN; 80 AML, 72 CLL, and 25 MDS/MPN; ref. 11). The highest frequency of APTO-253 sensitivity occurred in AML, with 43 of 80 (54 %) samples exhibiting an IC_{50} <1 μmol/L. At this cutoff, 25 of 72 CLL samples (35%) and 3 of 25 MDS/MPN samples (12%) were sensitive to APTO-253.

The goal of this project was to provide information on the mechanisms of action and resistance to APTO-253 so as to identify synthetic lethal interactions that can guide combination drug studies. We report here that APTO-253 is converted intracellularly into an Fe complex, and that this complex [Fe$(253)_3$] is likely the active form of the drug. Treatment of cells with APTO-253 generated DNA damage at early time points as documented by γ-H2AFX accumulation and foci formation. BRCA1- and BRCA2-deficient cells were found to be hypersensitive to APTO-253 to a degree comparable with that of olaparib. Resistance in Raji cells is associated with upregulation of the efflux transporter ABCG2, and resistance is partially reversed by ABCG2 inhibition. The ability of APTO-253 to exploit homologous recombination deficiency is of particular interest because, unlike all the other drugs for which loss of this repair function results in hypersensitivity, APTO-253 does not produce myelosuppression even at the MTD.

Materials and Methods

Drugs and reagents

APTO-253 and deuterated APTO-253 (APTO-253-d6) were provided by Aptose Biosciences. The chemical synthesis of APTO-253 is detailed in Supplementary Material. The DC™ Protein Assay was purchased from Bio-Rad Laboratories, Inc. PARP, MCL1, BAD, BIK, and ATP1A1 antibodies were from Cell Signaling Technology, Inc. pSer139-H2AFX (γ-H2AFX), total H2AFX, and ATM antibodies were purchased from Abcam. ABCG2 antibody was obtained from KAMIYA Biomedical. Ko143 (12) and pSer1981-ATM antibodies were obtained from Millipore Sigma. Olaparib was purchased from Selleckchem. Carboplatin and topotecan were obtained from UCSD Moores Cancer Center Pharmacy.

Cell types and culture

Raji and CAOV3 were obtained from the ATCC in 2015 and 2004. The APTO-253–resistant Raji (Raji/253R) cell line was generated by exposure to progressively higher concentrations of APTO-253 over a period of 6 months. MCF7 vector controlled and BRCA1 shRNA subclones were obtained from Dr. Simon Powell (Memorial Sloan-Kettering Cancer Center, New York, NY), and MCF10A and hTERT-IMEC clones were obtained from Dr. Ben Ho Park (Johns Hopkins University, Baltimore, MD) in 2016. HCT116 BRCA2$^{+/+}$ cells and BRCA2$^{-/-}$ cells were obtained from Dr. Samuel Aparicio (British Columbia Cancer Research Centre, Vancouver, Canada); PEO1 and PEO4 cells were obtained from Dr. Sharon Cantor (University of Massachusetts, Boston, MA), and HEK-293 pcDNA and ABCG2-transfected cells were obtained from Dr. Michael Gottesman (NIH, Bethesda, MD) in 2017. These cell lines were cultured under the same conditions as published previously (13–17). Early passage cells were collected and frozen within 1 month of receipt from the providers. All experiments were performed on early passage cells within 3 months of thawing. MycoAlert Plus Mycoplasma Detection Kit (Lonza) was used to screen for potential contamination, and the last screen was done on December 20, 2017. No authentication was done by the authors.

Cytotoxicity study

Cells were plated and treated with the indicated drugs in 96-well plates for 5 days. Cell viability was measured using CellTiter 96 AQ$_{ueous}$ one solution (MTS) cell proliferation assay purchased from Promega, and IC_{50} values were calculated using GraphPad Prism 6 software.

Biotinylation and immunoblotting procedure

To quantify ABCG2, expression cells were surface-biotinylated with EZ-LINK sulfo-NHS-SS-biotin (Thermo Fisher Scientific) and subjected to Western blot analysis as reported previously (18, 19).

RNA sequencing and qRT-PCR

Total cellular RNA was isolated using the RNeasy Mini Kit (QIAGEN) from three independent samples for each experiment. For RNA sequencing (RNA-seq), samples were submitted to the IGM Genomics Center, University of California, San Diego, La Jolla, CA (http://igm.ucsd.edu/genomics/) for library generation and validation using Agilent Bioanalyzer. Sequencing was performed on Illumina Sequencer HiSeq4000. Bioinformatic analysis was conducted by Oregon Health & Science University (Portland, OR). RNA-seq data were deposited to https://www.ncbi.nlm.nih.gov/geo/query/acc.cgi?acc=GSE111928 with the accession number GSE111928. Forward and reverse primers used for confirmation of ABCG2 overexpression were: 5'-TTA-GGA-TTG-AAG-CCA-AAG-G-3' and 5'-TAG-GCA-ATT-GTG-AGG-AAA-ATA-3', respectively.

Cellular pharmacology of APTO-253

Cells exposed to APTO-253 or Fe$(253)_3$ were homogenized in acetonitrile containing 5 ng of deuterated APTO-253 standard. Samples were analyzed at the UCSD Molecular Mass Spectrometry Facility employing an Agilent 1260 liquid chromatograph (LC) system coupled with a Thermo LCQdeca mass spectrometer using positive ion mode electrospray ionization (ESI) as the ion source. The ESI ion source voltage was set at 5 kV, with sheath gas flow rate of 80 U, auxiliary gas flow rate of 20 U, and capillary temperature of 250°C, respectively. A Phenomenex Kinetex Biphenyl column (ID 2.1 mm × length 50 mm, particle size 2.6 μm) was utilized for LC separation using water with 0.1% formic acid as the mobile phase A and acetonitrile with 0.1% formic acid as the mobile phase B. The LC flow rate was set at 0.30 mL/minute. The LC gradient increased from 5% mobile phase B to 95% mobile phase B in 10 minutes, held at 95% B for 2 minutes, returned to 5% B in 1 minute, and then held at 5% B for 6 minutes. Under positive ion mode ESI-MS/MS analysis, a major fragmental peak APTO-253 was observed at m/z 353 from its molecular ion peak at m/z 368 ([M+H]+) with a normalized collision energy of 45%, and a major fragmental peak of APTO-253-d6 at m/z 359 from its molecular ion peak at m/z 374 ([M+H]+) was observed with a normalized collision energy of 45%. Selected reaction monitoring (SRM) mode was used to acquire the m/z 353 and m/z 359 fragmental peaks. The SRM peak area ratio (APTO-253/APTO-253-d6) related to the amount of spiked APTO-253-d6 was used for the quantification of APTO-253 and Fe$(253)_3$ in the samples. The same column, gradient, and

flow rate were used for detection of $Fe(253)_3$, which was detected using an Agilent 1100 HPLC and Orbitrap XL (Thermo Fisher Scientific) mass spectrometer employing a Thermo Ion-Max ESI interface. The $Fe(253)_3$ eluted around 11.5 minutes with these conditions. A 10:1 flow split was used for the eluent flow rate of 0.3 mL/minute, so that approximately 0.030 mL/minute was introduced into the ESI after the split. The ion source MS parameters were as follows: capillary temperature 250°C, sheath gas flow 20 U, positive polarity, source voltage 5.0 kV, capillary voltage 22 V, and tube lens 80 V. The Fourier transform MS (Orbitrap) parameters were: FTMS AGC 1e6, FTMS microscans averaged 2, and FTMS full scan maximum ion time 500 ms. The resolution parameter of 15,000 (peak m/z divided by peak width given as full width at half maximum, at 400 m/z) was used. For the MS-MS CID spectra, a normalized collision energy of 45% was used.

Synthesis and characterization of $Fe(253)_3$

Five molar equivalents of ferrous ion as $FeSO_4$ in a concentrated water stock was added to APTO-253 in ethanol, which produced a deep red precipitate that was subsequently dissolved in DMSO and characterized by HPLC and mass spectrometry. $Fe(253)_3$ was >95 % pure and stable in the complete RPMI1640 media for at least 5 days.

Comet assay

Comet assay kits were purchased from Trevigen, and neutral comet assay was performed according to the manufacturer's instructions. Images were collected with a Keyence Fluorescent Microscope (Keyence America) and quantitated with OpenComet software.

Immunofluorescence staining

Cells were harvested, fixed in Z-fix solution (buffered zinc formalin fixatives, Anatech, Inc.), and permeabilized and blocked with 0.3% Triton X-100 in PBS containing 5% BSA. They were then incubated with γ-H2AFX antibody overnight followed by 1-hour incubation with fluorescent-conjugated secondary antibodies. Slides were mounted with ProLong Gold antifade reagent with 4′,6-diamidino-2-phenylindole (DAPI) to stain cell nuclei (Molecular Probes). Fluorescence was viewed with Keyence Fluorescent Microscope using a 100× objective and quantitated with FociCounter software.

Statistical analysis

All two-group comparisons utilized Student t test with the assumption of unequal variance. Data are presented as mean ± SEM of a minimum of three independent experiments.

Results

Cellular pharmacology of APTO-253

Among the cell types for which APTO-253 exhibits potent cytotoxicity, lymphomas are of interest as most of the standard chemotherapeutic agents used to treat this disease cause myelosuppression, which limits dose. For this reason, Raji Burkitt lymphoma cells were selected for study of the cellular pharmacology of APTO-253. The intracellular accumulation of APTO-253 in the Raji cells was quantified by LC/MS-MS. APTO-253 and its internal standard APTO-253-d6 eluted from the LC column at approximately 6.9 minutes with sharp peak profiles. Raji cells accumulated APTO-253 relatively slowly with content approaching steady state by 6 hours (Supplementary Fig. S1A).

Careful examination of the LC/MS-MS tracings identified a minor peak that eluted from the LC column at approximately 8.7 minutes under the same reaction monitoring mode selected for the detection of APTO-253. Using LC-HR-ESI-TOFMS (liquid chromatography high-resolution electrospray ionization time-of-flight mass spectrometry), a peak was identified with an m/z 578.65 that also eluted at approximately 8.7 minutes. High-resolution MS/MS analysis with the Obritrap MS demonstrated that this was a complex of APTO-253 with ferrous iron at 3-to-1 ratio (Fig. 1B). The structure of the $Fe(253)_3$ ternary complex was characterized by LC-MS-ESI. Two main features of the precursor ion mass spectrum constrained the identification of the structure. The first was the accurate mass measurement of the mass-to-charge ratio (m/z) of its positive two charged ion by high-resolution MS. The second feature was the isotope distribution of the measured peak that showed that the structure contained at least one atom of iron. In addition, the MS-MS spectrum of the complex showed two fragment ions, one at 368 m/z that was identical to the free APTO-253, and an ion at 789 m/z that was consistent with iron and two remaining APTO-253 ligands. The calculated mass of the ternary complex, 578.6520 m/z, was in very close agreement with the average m/z result observed on each of several different days, 578.6519 m/z. The difference ratio was −0.2 ppm, measured versus calculated. The interday SD was 0.0003 m/z, $n = 3$, and the intraday mass difference ratio was consistently less than 1.0 ppm. This measure of agreement is within the standard of 3 ppm, which is generally applied for proof of structure for synthetic organic products. The presence of iron was confirmed by the isotope pattern that is characteristic of that element. Iron has 4 stable isotopes, ^{54}Fe, ^{56}Fe, ^{57}Fe, and ^{58}Fe, with natural abundance of 5.85%, 91.75%, 2.12%, and 0.28%, respectively. The MS peak that occurs due to the ^{54}Fe isotope is distinctive because it does not coincide with natural isotopes of carbon, hydrogen, and nitrogen of the APTO-253 ligands. In the spectrum of the complex, its calculated mass is 577.6542 m/z (~1 m/z less than the most abundant isotope peak because the ion is charge plus two). The average mass observed for this peak was 577.6545 m/z, with SD 0.0003 m/z. The difference ratio was 0.5 ppm, interday with $n = 3$. The intensity of the ^{54}Fe peak also consistently measured about 6% of the ion abundance intensity of the main ^{56}Fe peak, as expected from the natural abundance ratio. For the measurement of the peak positions given above, the results were recalibrated with respect to an internal standard of 391.2843 m/z, an ion of diisooctyl phthalate that is ubiquitous due to ambient background.

We discovered that the $Fe(253)_3$ complex could be synthesized simply by adding $FeSO_4$ to APTO-253 in ethanol. The IC_{50} of $Fe(253)_3$ in the Raji cells was 145.7 ± 0.5 nmol/L, 1.5-fold less potent than APTO-253 presumably due to the difficulty of entering cells with its positive doubly charged Fe ion (Fig. 1C). The relative uptake of APTO-253 and $Fe(253)_3$ was examined by treating Raji cells with 0.5 μmol/L of each compound for 6 hours and correcting the intracellular concentrations on the basis of the ionization efficiency of each molecule (Fig. 1D). APTO-253–treated cells accumulated more intracellular $Fe(253)_3$ than the $Fe(253)_3$-treated cells, consistent with the difference in the IC_{50} of these two molecules.
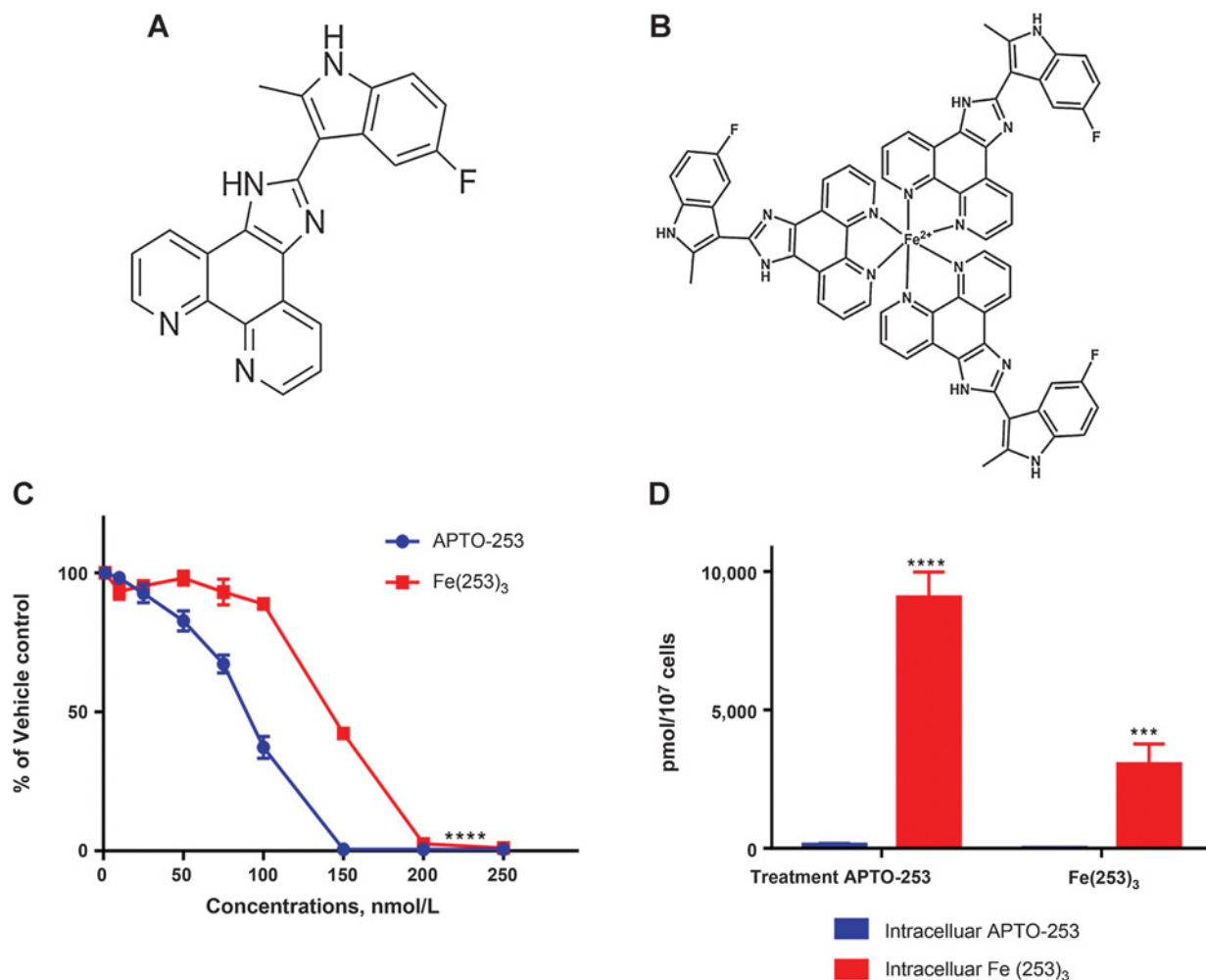
Figure 1.
Fe(253)$_3$ is an active intracellular form of APTO-253. **A,** Structure of APTO-253. **B,** Structure of Fe(253)$_3$. **C,** Relative cytotoxicity of APTO-253 (●) and Fe(253)$_3$ (■) in the Raji cells. **D,** The intracellular accumulation of APTO-253 (■) and Fe(253)$_3$ (■) in Raji cells exposed to 0.5 μmol/L APTO-253 or Fe(253)$_3$ for 6 hours. Vertical bars, ±SEM, where missing SEM is less than the size of the symbol. ***, $P < 0.001$; ****, $P < 0.0001$.

Although the majority of APTO-253 was converted to Fe(253)$_3$ intracellularly in the APTO-253–treated cells, Fe(253)$_3$ did not dissociate intracellularly to produce detectable free APTO-253 in the Fe(253)$_3$-treated cells. We concluded that Fe(253)$_3$ is the dominant active intracellular form of APTO-253.

APTO-253 causes DNA damage

The structure of APTO-253 is similar to drugs that bind to quadruplex structures in DNA, and work presented elsewhere indicates that APTO-253 does indeed bind quadruplex DNA *in vitro* and reduces the expression of Myc (20). The fact that such binding can produce strand breaks led us to investigate whether APTO-253 caused damage to DNA. The Raji cells were treated with 0.5 μmol/L APTO-253 for increasing periods of time, and induction of DNA damage was assessed by accumulation of the phosphorylated forms of ATM and γ-H2AFX measured by Western blot analysis. Figure 2A shows that APTO-253 produced a clear increase in phosphorylated ATM

and γ-H2AFX starting at 6 hours in Raji cells and that this increased with duration of drug exposure up to 24 hours. Cleavage of PARP was detected starting at 8 hours, indicating the induction of apoptosis. Raji cells have very small nuclei, making it difficult to quantify the formation of γ-H2AFX foci, so the human ovarian carcinoma cell line CAOV3, which has an IC$_{50}$ of 0.14 μmol/L, was used for this purpose. Figure 2B shows representative images of γ-H2AFX foci formation in the CAOV3 cells exposed to DMSO or 1 μmol/L APTO-253 for 24 hours. Figure 2C shows that an increase in the number of foci was detectable at 4 hours and that the number of foci increased more markedly after 8 hours. Evidence of DNA damage was further strengthened by the results of the neutral comet assay, which mainly detects DNA double-strand breaks (Fig. 2D). Although there was no increase in tail DNA when cells were treated with 0.5 μmol/L APTO-253 for 6 hours compared with the DMSO treatment, there was significantly more DNA in the comet tails when cells were treated with APTO-253 for 6 hours
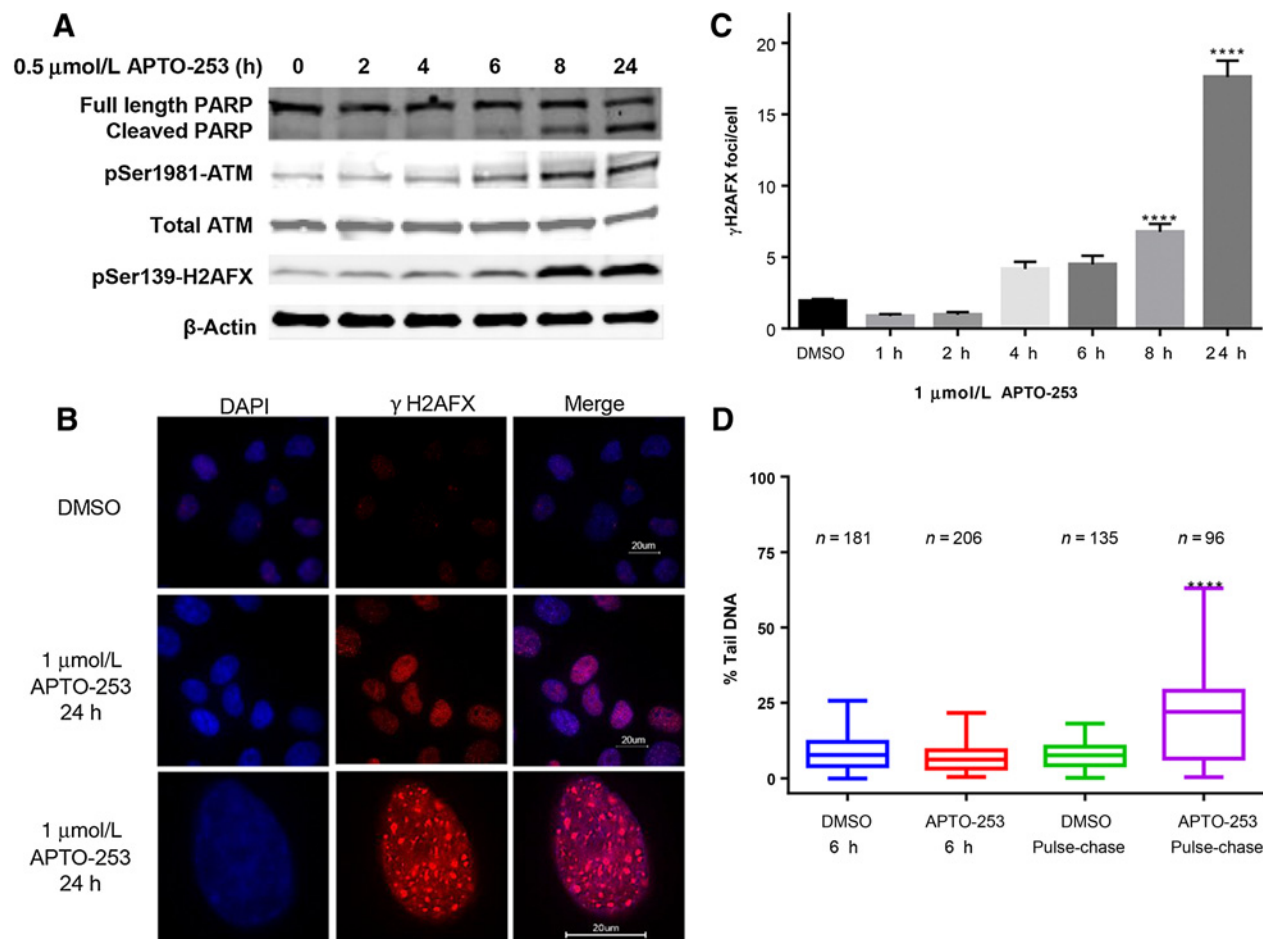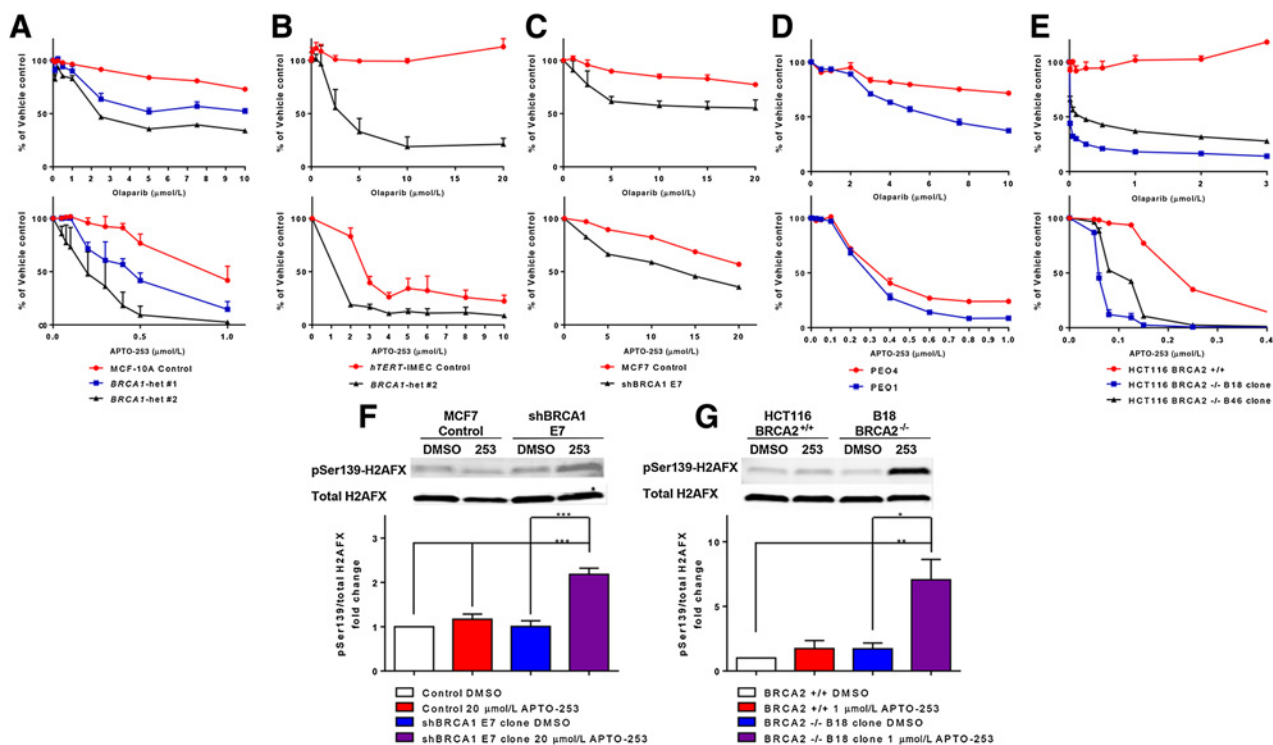
Figure 2.
APTO-253 causes DNA damage. **A,** The accumulation of phospho-ATM, phospho-H2AFX, and cleaved PARP in the Raji cells as a function of duration of exposure to 0.5 μmol/L APTO-253. The immunoblot shown is a representative of three independent experiments. **B,** Representative immunofluorescent images of nuclear foci formation comparing DMSO- and APTO-253–treated CAOV3 cells. **C,** Mean ± SEM number of γ-H2AFX foci per cell; $n = 100$. **D,** Box and whisker plot showing neutral comet assay quantification of percent tail DNA in Raji cells treated with DMSO or 0.5 μmol/L APTO-253 for 6 hours. n = number of cells examined; vertical bars, ±SEM. ****, $P < 0.0001$.

and then incubated in drug-free media for 18 hours (pulse-chase). These results provide strong evidence that APTO-253 generates DNA damage and produces accumulation of DNA strand breaks capable of triggering apoptosis.

BRCA1/2-deficient cells are hypersensitive to APTO-253

The finding that APTO-253 produced DNA damage led us to ask whether cells deficient in homologous recombination were hypersensitive to this drug. We tested the hypothesis that there would be synthetic lethality between APTO-253 and BRCA1 deficiency using isogenic pairs of BRCA1-proficient and -deficient human cell lines. Two independent MCF10A subclones, each containing a heterozygous knockin of a 2-bp deletion in BRCA1 that resulted in a premature termination codon (BRCA1-het #1 and #2), were found to be more sensitive to olaparib than clones that underwent random integration of the targeting vector within their genomes (control), confirming the loss of BRCA1 function in the two knockin clones (Fig. 3A, top). These two knockin clones were even more hypersensitive to APTO-253 than to olaparib (Fig. 3A, bottom). The effect of

impaired BRCA1 function was confirmed in a clone containing the same 2-bp knockin derived from the hTERT-IMEC cell line when it too was found to be hypersensitive to both olaparib and APTO-253 (Fig. 3B). The conclusion that BRCA1-deficient cells are hypersensitive to APTO-253 was further supported by the results obtained in MCF7 E7 cells in which BRCA1 expression is stably knocked down by the expression of an shRNAi (13). As shown in Fig. 3C, the E7 clone has a similar degree of hypersensitivity toward olaparib and APTO-253. These results in 3 independent isogenic pairs of BRCA1-competent and incompetent cells indicate that repair of the DNA damage produced by APTO-253 is in part dependent on homologous recombination and/or other DNA repair pathways in which BRCA1 functions. Whether BRCA2-deficient cells are more sensitive to APTO-253 was tested using BRCA2-proficient and -deficient ovarian cancer cell lines, PEO4 and PEO1. PEO1 is BRCA2 deficient and sensitive to cisplatin and a PARP inhibitor AG14361. PEO4 was derived from ascites at the time of relapse with cisplatin resistance and contains a secondary mutation that restores BRCA2 function (14). Restoration of BRCA2

Figure 3.
Loss of BRCA1 and BRCA2 function results in hypersensitivity to APTO-253. Sensitivity of BRCA1-proficient and -deficient isogenic MCF10A clones (**A**), *hTERT*-IMEC clones (**B**), and MCF7 (**C**) to olaparib (top) and APTO-253 (bottom). Sensitivity of BRCA2-proficient and -deficient isogenic PEO4 and PEO1 (**D**), and HCT116 BRCA2-deficient clones (**E**) to olaparib (top) and APTO-253 (bottom). The accumulation of γ-H2AFX in the MCF7 control and shBRCA1 clone E7 cells (**F**) and the BRCA2-proficient HCT116 and the deficient clone B18 cells treated with DMSO or the indicated concentration of APTO-253 for 24 hours (**G**). Vertical bars, ±SEM. *, $P < 0.05$; **, $P < 0.01$; ***, $P < 0.001$.

function increased resistance to both olaparib (Fig. 3D, top) and APTO-253 (Fig. 3D, bottom). Similar results were obtained using the BRCA2-proficient HCT116 cells and 2 BRCA2$^{-/-}$ subclones, B18 and B46 (Fig. 3E). Thus, loss of either BRCA1 or BRCA2 function renders malignant cells hypersensitive to APTO-253. The mechanism of the hypersensitivity was further examined by treating parental MCF7 cells and the BRCA1-deficient MCF7 subline shBRCA1 E7 with 20 µmol/L APTO-253 for 24 hours. As shown in Fig. 3F, there was 2.2 ± 0.14-fold more γ-H2AFX accumulation in the MCF7/shBRCA1 E7 cells ($n = 3$). Similar results were also found in a comparison of parental HCT116 cells and the BRCA2-deficient B18 clone of HCT116 when they were treated with 1 µmol/L APTO-253. There was 7.1 ± 0.16-fold more γ-H2AFX accumulation in the BRCA2$^{-/-}$ B18 cells (Fig. 3G, $n = 3$). These results further support the importance of BRCA1 and 2 to repair the DNA damage generated by APTO-253.

Selection for acquired drug resistance

To delineate which effects of APTO-253 are most closely linked to sensitivity for this drug, we took the approach of developing a subline of the Raji Burkitt lymphoma cell line that had acquired resistance (Raji/253R). Resistance evolved slowly and progressively without an abrupt change at any point during the selection process. The IC$_{50}$ of APTO-253 for the parental Raji cells was 105.4 ± 2.4 nmol/L when tested using an assay that quantified growth rate during a 120-hour exposure to drug.

This is in the same range as has been reported for freshly isolated AML blasts and CLL cells (9, 11). The Raji/253R cells were 16.7 ± 3.9-fold resistant to APTO-253 (IC$_{50}$: 1,387.7 ± 98.5 nmol/L). The level of resistance remained stable for at least 3 months during culture in drug-free media (Fig. 4A). Raji/253R cells grew slightly faster than the parental cells, but the difference was not statistically significant. At a concentration that induced apoptosis in the Raji-sensitive cells, APTO-253 failed to trigger apoptosis in the Raji/253R cells. When the sensitive cells were treated with 0.5 µmol/L APTO-253 for 24 hours, the proapoptotic proteins BIK and BAD increased by 47.5 ± 16.8% and 2.1 ± 0.25-fold, respectively ($P < 0.05$, $n = 3$) and the antiapoptotic protein MCL1 decreased by 38.1 ± 2.3% ($P < 0.001$, $n = 3$) compared with the DMSO control. None of these changes were detected in the Raji/253R cells subjected to the same exposure (Fig. 4B).

Mechanism of drug resistance

Resistance in the Raji/253R cells may be due to alterations in influx or efflux, intracellular detoxification, a change in the primary target of the drug, or altered regulation of DNA repair mechanisms. We monitored the intracellular accumulation of both native APTO-253 and the Fe(253)$_3$ in Raji and Raji/253R cells incubated with either native APTO-253 or the Fe(253)$_3$ complex. These results indicate that resistance to APTO-253 in Raji cells is associated with impaired accumulation of both forms of the drug; however, the level of the Fe(253)$_3$ complex still
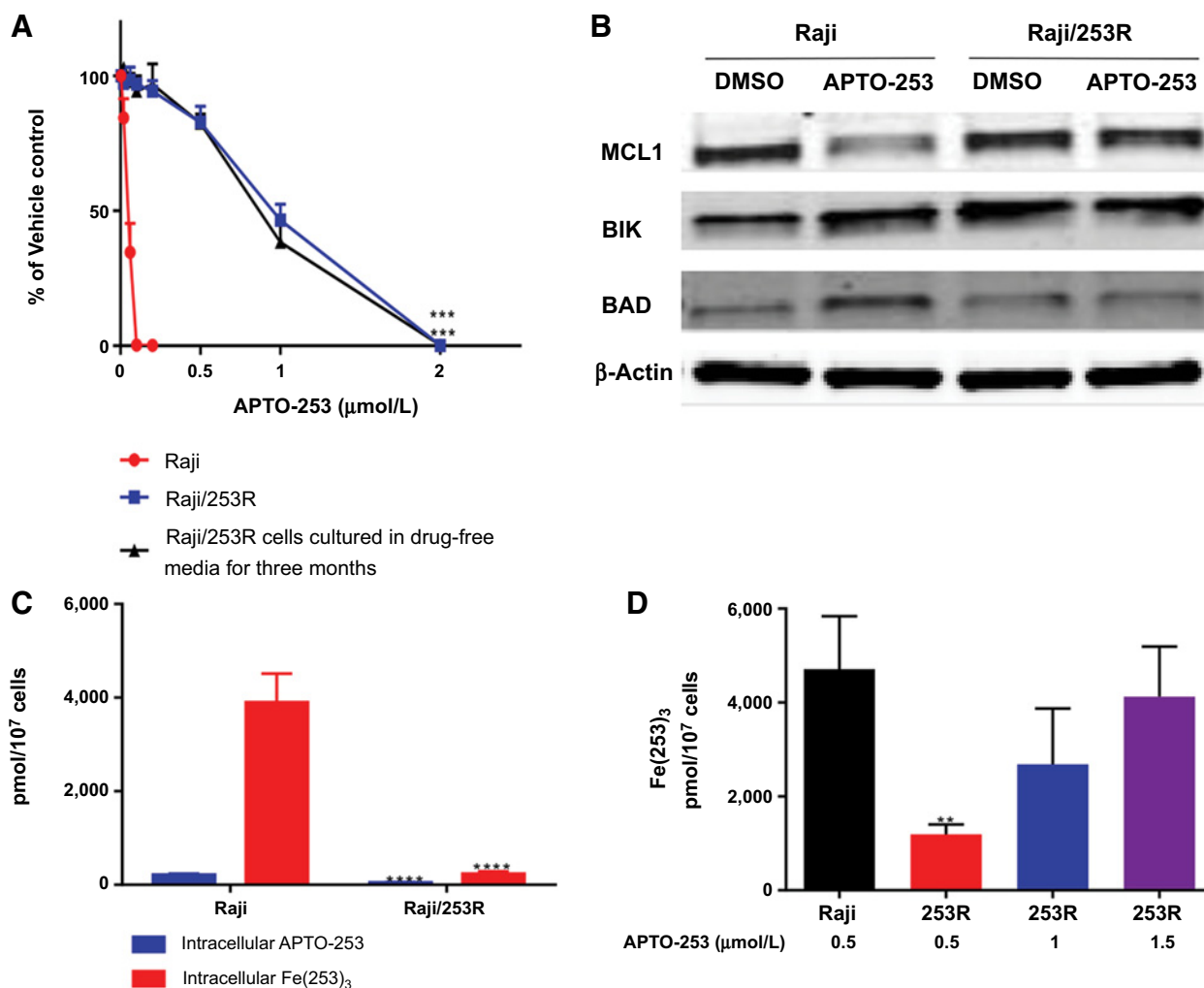
Figure 4.
Characterization of cells resistant to APTO-253. **A,** Concentration–survival curves for Raji (●), Raji/253R (■), Raji/253R, and Raji/253R cells after culture in drug-free medium for 3 months (▲). **B,** Western blot analysis of proteins involved in apoptosis in Raji and Raji/253R treated with DMSO or APTO-253 0.5 μmol/L for 24 hours. **C,** The intracellular accumulation of APTO-253 (■) and Fe(253)$_3$ (■) in Raji and Raji/253R cells after a 6-hour exposure to 0.5 μmol/L APTO-253. **D,** The intracellular accumulation of Fe(253)$_3$ in the Raji and Raji/253R cells at 6 hours as a function of APTO-253 concentration. Vertical bars, ±SEM. ** $P < 0.01$; ***, $P < 0.001$; ****, $P < 0.0001$.

exceeded that of the native drug (Fig. 4C). Only when the Raji/253R cells were treated with at least 3 times as much APTO-253 did the intracellular content of Fe(253)$_3$ finally reach a level similar to that in the sensitive cells (Fig. 4D). The rate of accumulation of both forms of the drug was severely reduced in the Raji/253R cells exposed to APTO-253 (Supplementary Fig. S1A). The same was true to lesser extent when the cells were incubated with the Fe(253)$_3$ complex (Supplementary Fig. S1B). In contrast, there was no apparent difference in the efflux over the first 2 hours of either APTO-253 or Fe(253)$_3$ following loading of the cells with either form of the drug (Supplementary Fig. S1C; Supplementary Table S1). Treatment of the Raji/253R cells with 0.5 μmol/L APTO-253 for 24 hours produced no increase in phospho-ATM or phospho-H2AFX, and no detectable PARP cleavage (Supplementary Fig. S2) consistent with substantially less intracellular APTO-253 and Fe(253)$_3$ in the resistant cells.

To obtain further insight into the resistance mechanism, RNA-seq analysis was carried out on three independent samples of both the sensitive Raji and resistant Raji/253R cells. A gene-level differential expression analysis was performed by removing all genes with less than 50 reads across all 6 samples, as genes with only low-level expression can cause irregularities in differential expression analysis. Genes were considered to be differentially expressed if their adjusted P value was less than the 0.05 level and their fold change was >2 in either direction. Among the 13,791 evaluable genes, there were 1,012 that were significantly upregulated in the Raji/253R cells and 704 genes that were significantly downregulated relative to the parental sensitive Raji cells. The ATP-binding cassette subfamily member ABCG2 was the most upregulated gene with more than a thousand-fold increase in transcript level (Supplementary Table S2). Although several other multidrug resistance ABC
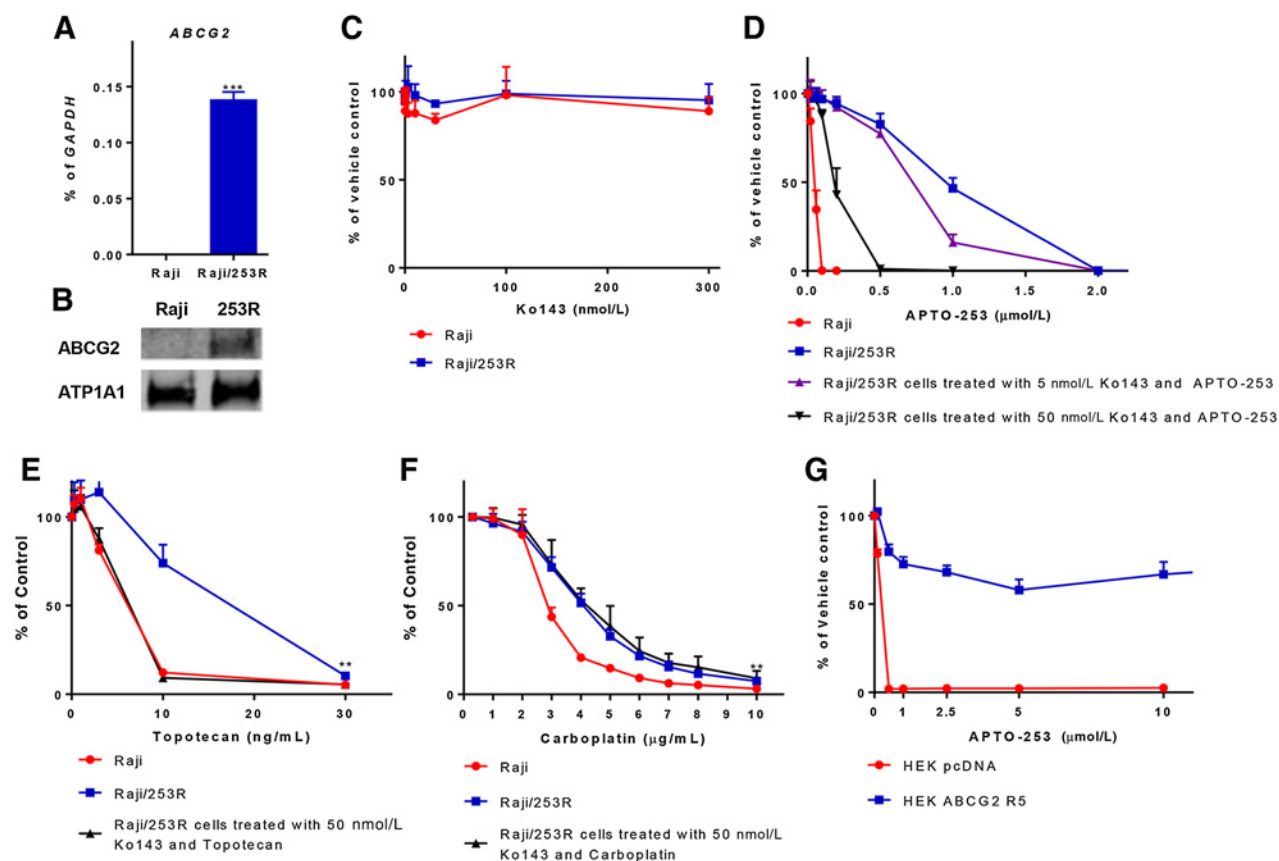
Figure 5.
Role of ABCG2 in resistance to APTO-253. **A,** Relative levels of ABCG2 mRNA in Raji and Raji/253R. **B,** Western blots of biotinylated proteins were probed with anti-ABCG2 antibody. ATP1A1 served as a loading control. **C,** Cytotoxicity of Ko143 in Raji (●) and Raji/253R (■). **D,** Concentration–survival curves for Raji (●) and Raji/253R (■) treated with APTO-253 alone or in combination with APTO-253 and 5 nmol/L (▲) or 50 nmol/L Kol43 (▼). **E,** Cytotoxicity of topotecan in Raji (●) and Raji/253R (■) and the combination of topotecan and 50 nmol/L Ko143 in Raji/253R (▲). **F,** Cytotoxicity of carboplatin in Raji (●) and Raji/253R (■) and the combination of carboplatin and 50 nmol/L Ko143 in Raji/253R (▲). **G,** Concentration–survival curves for HEK-293 transfected with pcDNA (●) and ABCG2, clone R5 (■) treated with APTO-253. Vertical bars, ± SEM. **, $P < 0.01$; ***, $P < 0.001$.

transporters were also upregulated in Raji/253R, the increase in ABCG2 transcripts was the most prominent (Supplementary Table S3). The marked upregulation of ABCG2 in the Raji/253R cells was confirmed by qRT-PCR and Western blot analysis (Fig. 5A and B).

Ko143 is a specific ABCG2 inhibitor with more than 200-fold selectivity relative to its ability to inhibit the P-gp or MRP-1 transporters (12). Ko143 itself was not toxic to Raji or Raji/253R cells at concentrations up to 300 nmol/L (Fig. 5C). To test the hypothesis that APTO-253 is a substrate for ABCG2, we determined the ability of Ko143 to reverse the resistance of the Raji/253R cells. The data in Table 1 and Fig. 5D show that concurrent treatment with Ko143 significantly reversed APTO-253 resistance only in the Raji/253R cells, but had no effect on sensitivity to APTO-253 in Raji cells. Ko143 also reversed Fe $(253)_3$ resistance in the Raji/253R cells, further confirming that the upregulation of ABCG2 is one of the main mechanisms of APTO-253 resistance (Supplementary Fig. S3A). To provide further evidence of augmented ABCG2 function, the resistant cells were tested for cross-resistance to topotecan, a well-documented

Table 1. Effect of ABCG2 inhibitor on resistance to APTO-253

Cell line	APTO-253 alone		APTO-253 + 5 nmol/L Ko143		APTO-253 + 50 nmol/L Ko143	
	IC$_{50}$ (nmol/L)[a]	RR[b]	IC$_{50}$ (nmol/L)	RR[b]	IC$_{50}$ (nmol/L)	RR[b]
Raji/253R	1,387 ± 94	16.7 ± 3.9[c]	853 ± 44	10.9 ± 1.9[d]	200.6 ± 20.7	2.5 ± 0.7[e]
Raji	105 ± 2.4	—	98.3 ± 0.8	—	103.1 ± 2.9	—

[a]Mean ± SEM.
[b]Relative resistance.
[c]$P < 0.01$.
[d]$P < 0.001$.
[e]$P < 0.05$.

ABCG2 substrate. The Raji/253R cells were found to be 3-fold cross-resistant to topotecan, and treatment with Ko143 reversed this resistance completely (Fig. 5E). Intriguingly, Raji/253R was also significantly cross-resistant to carboplatin even though carboplatin is not thought to be an ABCG2 substrate; treatment with Ko143 did not reduce the carboplatin IC_{50} in the Raji/253R cells (Fig. 5F). Finally, ABCG2-overexpressing HEK-293 cells were much more resistant to both APTO-253 and $Fe(253)_3$ treatment with IC_{50} values of >10 μmol/L when the IC_{50} values for the parental cells 139.6 ± 3.6 and 252.3 ± 14.4 nmol/L for APTO-253 and $Fe(253)_3$, respectively (Fig. 5G; Supplementary Fig. S3B). Collectively, these data illustrate a role for the ABCG2 efflux transport system in the resistance to APTO-253.

Discussion

APTO-253 is of interest because it is a member of a novel class of compounds that exhibits cytotoxicity against a wide range of malignancies and does not cause myelosuppression. The first key finding reported here is that the APTO-253 monomer is converted intracellularly to an active complex containing a ferrous Fe atom and 3 molecules of APTO-253 whose intracellular concentration exceeds that of the native drug. The second key finding is that the evidence supports $Fe(253)_3$ as the active form of the drug. The third key finding is that treatment of cells with APTO-253 leads to DNA damage; it was this observation that led to the fourth key finding that repair of the APTO-253–induced DNA damage requires the function of both BRCA1 and BRCA2, as evidenced by synthetic lethality with APTO-253. In the case of Raji cells, acquired resistance is associated with reduced drug uptake and marked overexpression of the ABCG2 drug efflux pump whose inhibition partially reverses resistance, and there is the suggestion of a role of modified DNA repair mechanisms in the resistant cells because the Raji/253R cells are cross-resistant to carboplatin.

As APTO-253 begins to accumulate intracellularly in the Raji cells, it is rapidly converted to $Fe(253)_3$ as this complex is present as soon as the native form of the drug is detected in the cell. By 6 hours, the cellular content of the $Fe(253)_3$ exceeded that of the native form by approximately 18-fold. The potency of the $Fe(253)_3$ complex is only 1.5-fold less than that of native drug, which can be accounted for by the fact that, although APTO-253 is neutral, $Fe(253)_3$ is much larger and contains a 2^+ charge, which would be expected to impair transmembrane influx. The fact that no native drug was detectable in cells incubated with the $Fe(253)_3$ complex strongly suggests that $Fe(253)_3$ is the active intracellular form of the drug. Drugs containing the 2,10 indole ring structure are known to chelate Fe and Zn. In the case of APTO-253, although the Fe chelate was abundant in cells, a Zn chelate was not detectable. The high level of $Fe(253)_3$ raises the question of whether its formation depletes critical cellular proteins of Fe to the point where cellular metabolism is impaired, and this remains an interesting point for further investigation.

APTO-253 causes DNA damage as evidenced by an increase in phosphorylated ATM and γ-H2AFX, γ-H2AFX foci formation, and DNA fragmentation. These observations led to the discovery that the cells deficient in either BRCA1 or BRCA2 are hypersensitive to APTO-253. The observation that deficiency in homologous recombination results in hypersensitivity to certain types of DNA-damaging drugs has been exploited to

increase the effectiveness of the platinum-containing drugs and the PARP inhibitors particularly in the case of ovarian cancer (21, 22). APTO-253 joins the limited repertoire of drugs that can take advantage of this important therapeutic window. Isogenic paired repair-proficient and -deficient cell lines provide powerful tools with which to assess the role of DNA repair processes, and the finding of hypersensitivity to APTO-253 across multiple such pairs constitutes strong evidence that APTO-253 causes DNA damage and that the type of damage produced is subject to BRACA1/2-mediated repair. The observations reported here identify γ-H2AFX as a potential biomarker of clinical drug effect and point the way toward more detailed studies of how APTO-253 causes DNA damage (23). One of the issues to be addressed is whether deficiencies in other types of DNA repair might also render cells hypersensitive to APTO-253.

Development of acquired resistance to APTO-253 in the Raji lymphoma cells was associated with reduced accumulation of APTO-253 and the $Fe(253)_3$ complex. There was 16.5 ± 1.94-fold more intracellular $Fe(253)_3$ in the Raji-sensitive cells than the resistant cells, which corresponds well to the relative resistance of the Raji/253R over the sensitive cells (16.7 ± 3.9-fold). RNA-seq analysis of the Raji/253R cells pointed most directly to overexpression of ABCG2 as a possible mechanism of resistance. Western blot analysis confirmed upregulation at the protein level, and that ABCG2 was functional and directly involved in APTO-253 resistance was established by the ability of its inhibitor to partially reverse resistance to APTO-253 as well as $Fe(253)_3$. None of the known classes of drugs for which increased ABCG2 confers resistance have obvious structural similarity to APTO-253 or $Fe(253)_3$. Thus, the discovery that ABCG2 can mediate resistance to APTO-253 expands the range of known substrates for this important transporter. Whether ABCG2 can be used as a biomarker for sensitivity to APTO-253 will need to be explored in a large panel of cell lines. Nevertheless, we have identified an intracellular form of APTO-253 as the putative active form of the drug and have shown that the drug acts through promotion of DNA damage and is synthetically lethal with BRCA1/2 deficiencies in cancer cells.

Authors' Contributions

Conception and design: C.-Y. Tsai, H. Zhang, W.G. Rice, S.B. Howell
Development of methodology: C.-Y. Tsai, H. Zhang, Y. Su, S.B. Howell
Acquisition of data (provided animals, acquired and managed patients, provided facilities, etc.): C.-Y. Tsai, S. Sun, Y. Su
Analysis and interpretation of data (e.g., statistical analysis, biostatistics, computational analysis): C.-Y. Tsai, S. Sun, A. Local, Y. Su, L.A. Gross, W.G. Rice, S.B. Howell
Writing, review, and/or revision of the manuscript: C.-Y. Tsai, H. Zhang, W.G. Rice, S.B. Howell
Administrative, technical, or material support (i.e., reporting or organizing data, constructing databases): C.-Y. Tsai
Study supervision: S.B. Howell

Tsai et al.

References

1. Mudasir, Wijaya K, Yoshioka N, Inoue H. DNA binding of iron(II) complexes with 1,10-phenanthroline and 4,7-diphenyl-1,10-phenanthroline: salt effect, ligand substituent effect, base pair specificity and binding strength. J Inorg Biochem 2003;94:263–71.

2. Mudasir, Wijaya K, Wahyuni ET, Inoue H, Yoshioka N. Base-specific and enantioselective studies for the DNA binding of iron(II) mixed-ligand complexes containing 1,10-phenanthroline and dipyrido[3,2-a:2′,3′-c]phenazine. Spectrochimica acta Part A, Mol Biomol Spect 2007;66: 163–70.

3. Mudasir, Yoshioka N, Inoue H. Enantioselective DNA binding of iron(II) complexes of methyl-substituted phenanthroline. J Inorg Biochem 2008; 102:1638–43.

4. Mudasir, Yoshioka N, Inoue H. DNA binding of iron(II) mixed-ligand complexes containing 1,10-phenanthroline and 4,7-diphenyl-1,10-phenanthroline. J Inorg Biochem 1999;77:239–47.

5. Huesca M, Lock LS, Khine AA, Viau S, Peralta R, Cukier IH, et al. A novel small molecule with potent anticancer activity inhibits cell growth by modulating intracellular labile zinc homeostasis. Mol Cancer Ther 2009; 8:2586–96.

6. Cukier H, Peralta R, Jin H, Cheng Y, Nedunuri V, Salehi S, et al. Utilization of KLF-4 as a pharmacodynamic biomarker for *in vivo* anticancer activity of a novel small molecule drug LOR-253 [abstract]. In: Proceedings of AACR 104th Annual Meeting 2013; 2013Apr 6–10; Washington, DC. Philadelphia (PA): AACR; 2013. Abstract nr 4649.

7. Cercek A, Wheler J, Murray PE, Zhou S, Saltz L. Phase 1 study of APTO-253 HCl, an inducer of KLF4, in patients with advanced or metastatic solid tumors. Invest New Drugs 2015;33:1086–92.

8. Lum R, Javadi M, Cheng T, Peralta R, Cukier H, Lightfoot J, et al. Induction of KLF4 by LOR-253 as an innovative therapeutic approach to induce apoptosis in acute myueloid leukemia [abstract]. In: Proceedings of the 105th Annual Meeting of the American Association for Cancer Research; 2014 Apr 5–9; San Diego, CA. Philadelphia (PA): AACR; 2014 Abstract nr 4544.

9. Zhang H, Local A, Benbatoul K, Folger P, Sheng S, Esquivies L, et al. Inhibition of c-Myc by APTO-253 as an innovative therapeutic approach to induce cell cycle arrest and apoptosis in acute myeloid leukemia [abstract]. Blood 2016;128:1716.

10. Wang B, Shen A, Ouyang X, Zhao G, Du Z, Huo W, et al. KLF4 expression enhances the efficacy of chemotherapy drugs in ovarian cancer cells. Biochem Biophys Res Commun 2017;484:486–92.

11. Kurtz SE, Bototmly D, Wilmont B, McWeeney SK, Rice WG, Howell SB, et al. Broad activity of APTO-253 in AML and other hematologic

12. Liu K, Zhu J, Huang Y, Li C, Lu J, Sachar M, et al. Metabolism of KO143, an ABCG2 inhibitor. Drug Metab Pharmacokinet 2017;32: 193–200.

13. Fridlich R, Annamalai D, Roy R, Bernheim G, Powell SN. BRCA1 and BRCA2 protect against oxidative DNA damage converted into double-strand breaks during DNA replication. DNA Repair 2015;30:11–20.

14. Sakai W, Swisher EM, Jacquemont C, Chandramohan KV, Couch FJ, Langdon SP, et al. Functional restoration of BRCA2 protein by secondary BRCA2 mutations in BRCA2-mutated ovarian carcinoma. Cancer Res 2009;69:6381–6.

15. Konishi H, Mohseni M, Tamaki A, Garay JP, Croessmann S, Karnan S, et al. Mutation of a single allele of the cancer susceptibility gene BRCA1 leads to genomic instability in human breast epithelial cells. Proc Natl Acad Sci U S A 2011;108:17773–8.

16. Xu H, Di Antonio M, McKinney S, Mathew V, Ho B, O'Neil NJ, et al. CX-5461 is a DNA G-quadruplex stabilizer with selective lethality in BRCA1/2 deficient tumours. Nat Commun 2017;8:14432.

17. Robery R, Honjo Y, Morisaki K, Nadjem T, Runge S, Risbood M, et al. Mutations at amino-acid 482 in the ABCG2 gene affect substrate and antagonist specificity. Br J Cancer 2003;89:1971–8.

18. Tsai CY, Finley JC, Ali SS, Patel HH, Howell SB. Copper influx transporter 1 is required for FGF, PDGF and EGF-induced MAPK signaling. Biochem Pharmacol 2012;84:1007–13.

19. Tsai CY, Liebig JK, Tsigelny IF, Howell SB. The copper transporter 1 (CTR1) is required to maintain the stability of copper transporter 2 (CTR2). Metallomics 2015;7:1477–87.

20. Local A, Zhang H, Benbatoul K, Folger P, Sheng S, Tsai CY, et al. APTO-253 interaction with G-Quadruplex DNA is linked to inhibition of c-Myc expression, induction of DNA damage, and generation of synthetic lethality in cells with BRCA1/2 Impairment. Blood 2017; 130:5094.

21. Ledermann J, Harter P, Gourley C, Friedlander M, Vergote I, Rustin G, et al. Olaparib maintenance therapy in platinum-sensitive relapsed ovarian cancer. N Engl J Med 2012;366:1382–92.

22. Mirza MR, Monk BJ, Herrstedt J, Oza AM, Mahner S, Redondo A, et al. Niraparib maintenance therapy in platinum-sensitive, recurrent ovarian cancer. N Engl J Med 2016;375:2154–64.

23. Ivashkevich A, Redon CE, Nakamura AJ, Martin RF, Martin OA. Use of the gamma-H2AX assay to monitor DNA damage and repair in translational cancer research. Cancer Lett 2012;327:123–33.

Molecular Cancer Therapeutics

APTO-253 Is a New Addition to the Repertoire of Drugs that Can Exploit DNA BRCA1/2 Deficiency

Cheng-Yu Tsai, Si Sun, Hongying Zhang, et al.

Updated version	Access the most recent version of this article at: doi:10.1158/1535-7163.MCT-17-0834
Supplementary Material	Access the most recent supplemental material at: http://mct.aacrjournals.org/content/suppl/2018/04/06/1535-7163.MCT-17-0834.DC1 http://mct.aacrjournals.org/content/suppl/2018/04/13/1535-7163.MCT-17-0834.DC2

E-mail alerts	Sign up to receive free email-alerts related to this article or journal.
Reprints and Subscriptions	To order reprints of this article or to subscribe to the journal, contact the AACR Publications Department at pubs@aacr.org.
Permissions	To request permission to re-use all or part of this article, use this link http://mct.aacrjournals.org/content/early/2018/05/14/1535-7163.MCT-17-0834. Click on "Request Permissions" which will take you to the Copyright Clearance Center's (CCC) Rightslink site.